layer may be persisted in this area. Areas with likely more dynamic activity often correlate with areas lacking nodules. These include sediment drifts and exposed basalt/carbonate. In the case of sediment drifts, the adjacent nodule fields are composed of a few large to very large nodules (Figure 7.35). In the case of exposed rock surfaces (typically near scarp edges; Figure 7.34), smaller nodules are found and in some cases nodules are seen sitting on the rock with sediments winnowed away.

The conditions supporting nodule formation must have been present for most of their long period of slow growth. For some nodules growth rates look to have been consistent (Figure 7.26), but in other nodules they may have been less so. Examples of this could be in areas with consistently (slightly) higher currents and in areas with more ephemeral conditions (e.g. dependent upon climate/plankton blooms or periodic changes in current). Areas with a medium to thin geochemical layer that waxes and wanes might form irregular small to medium sized nodules. Areas with periodic influx of material might form a few larger nodules. Areas of mixed large and small nodules might develop when an area with large nodules (and thicker geochemically active layer) transforms into an area with a consistently thinner geochemically active layer. Certainly it seems likely that larger nodules, with their much greater surface area, would absorb more new metal (i.e., outcompete) than nearby smaller nodules. In some cases nodules fragment and form the core of new nodules (e.g. as suggested by Sorem and Fewkes, 1977 and Halbach and Özkara, 1979).

The thickness of the geochemically active layer is almost certainly related in part to the host or base sediment type. Within the CCZ both siliceous and calcareous oozes have been identified (Kotlinski, 2003), and between the different TOML sub areas there appears to be both primary and residual calcareous ooze, with the later, frequently coarser grained sediment, forming from degraded Marquesas Formation. It is also worth noting that based on Fe/Mn ratios, many of the smaller smoother-skinned nodules found in the TOML areas are still mostly diagenetic in nature (see further below). Some nodules collected by TOML show clear evidence of overturning with glazed over crenulated former bases and roughened botryoidal former tops. The mechanisms for nodules to be turned might include biological activity (e.g. undermining by burrowing).

Table 7.6 Interpreted outcome of thickness vs stability of geochemically active layer

Geochemically active layer	Very thick	Thick	Med	Thin to None
Stable	Very large nodules e.g. SW TOML area D1, Figure 7.31	Large nodules e.g. central TOML field B5338	Medium sized nodules e.g. TOML area C1, Figure 7.31	Small and more hydrogenetic nodules e.g. edges of TOML field B5338 or on exposed basalt/carbonate e.g. Figure 7.34
Unstable	Marginal to Nnoo few rare nodules of large or uneven size e.g. Figure 7.35	e.g., torpedoes on slopes (grow faster in direction of flow e.g. Figure 7.33	Irregular sized nodules e.g. Figure 7.32	
Dynamic	Nodules cannot form either hard surface or sediment only (unit Nnoo)			

Figure 7.31 Example high density of larger and smaller sized nodules, illustrating near space arrangement and bioturbation

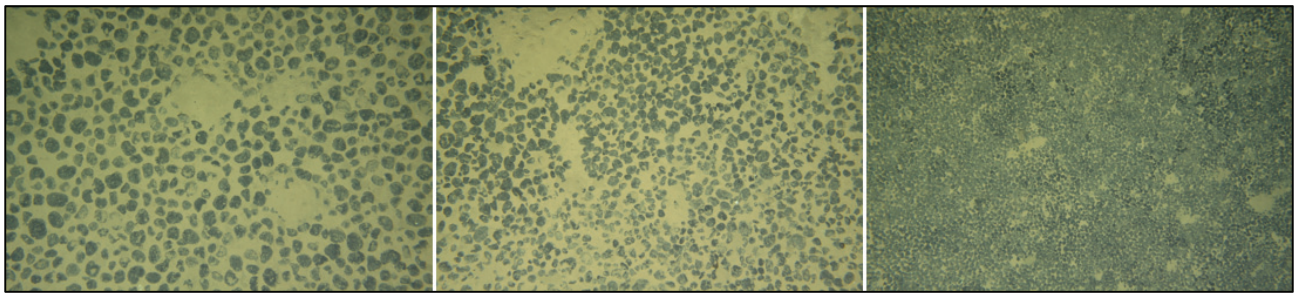

Photos: 2.4 x 1.5 m; L->R: F02 - 2015_08_17_034820 - F01 - 2015_08_11_114315 - F02 - 2015_08_16_180644

Figure 7.32 Examples of irregular nodule sizes – note bioturbation around some larger nodules

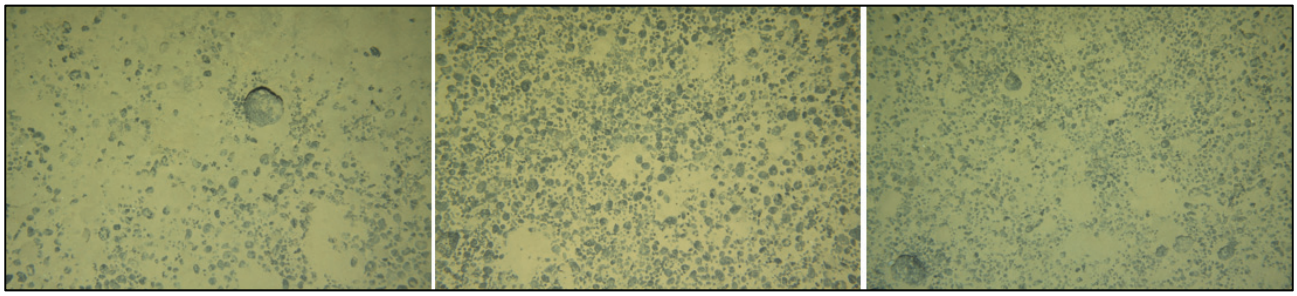

Photos: 2.4 x 1.5 m; L->R: F02 - 2015_08_17_122525 - F01 - 2015_08_11_065901 - F02 - 2015_08_16_190032

Figure 7.33 Example holothurian sweeping and aligned prolate nodules

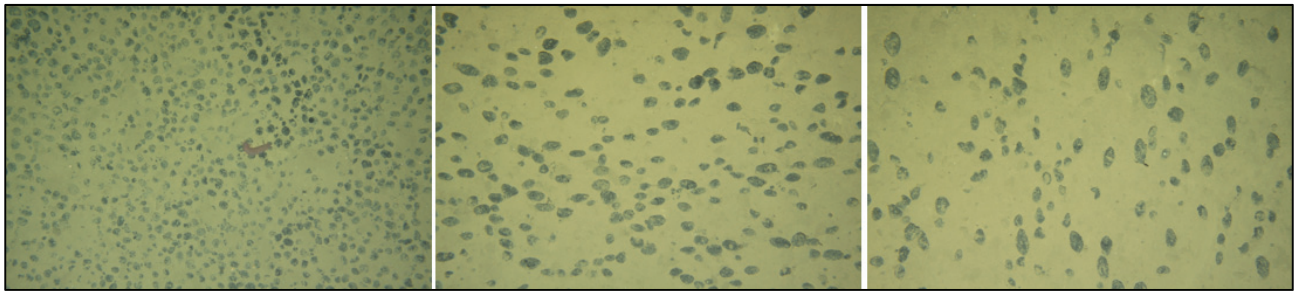

Photos: 2.4 x 1.5 m; L->R: - F01 - 2015_08_10_123744 - F01- 2015_08_11_023739 - F01 - 2015_08_11_024926

Figure 7.34 Examples of small nodules in thin sediment amongst basalt and carbonate

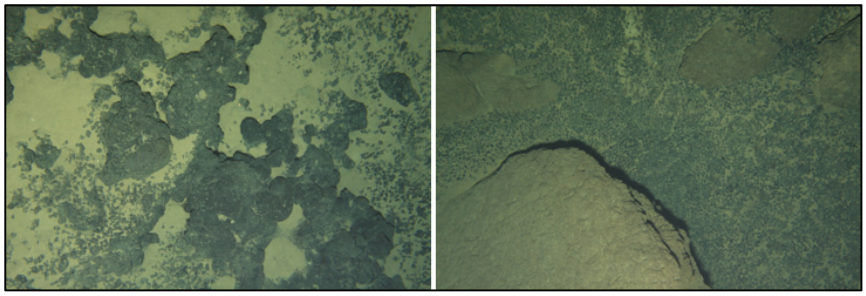

Photos: 2.4 x 1.5 m; L->R: F02 - 2015_08_17_092409 - F02 - 2015_08_16_184149

Figure 7.35 Examples of ooze without nodules, grading to reappearance

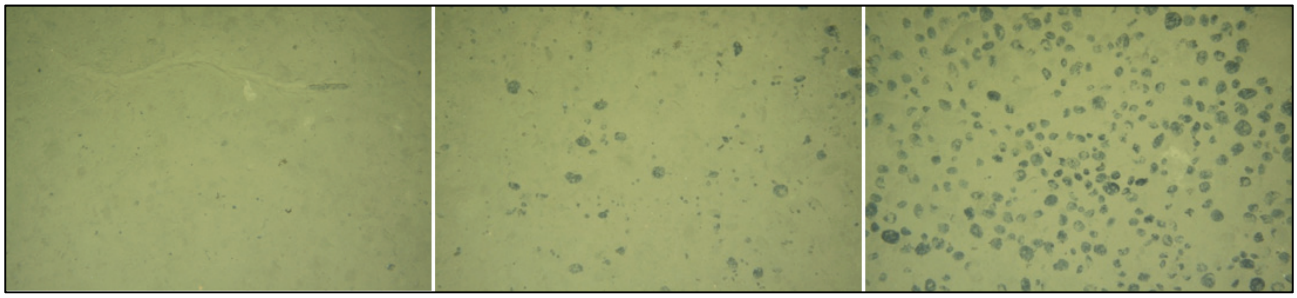

Photos: 2.4 x 1.5 m; L->R: F03 - 2015_08_22_010706 - 2015_08_22_033727 - 2015_08_22_034104

Figure 7.36 Examples of high rates of powder-cover

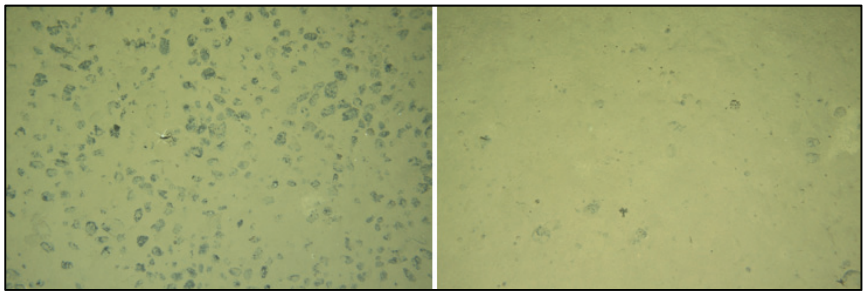

Photos: 2.4 x 1.5 m; L->R: F09B - 2015_09_15_064553 F09B - 2015_09_15_071239

Figure 7.37 Examples of basalt fragments; same on carbonate; in a box-core

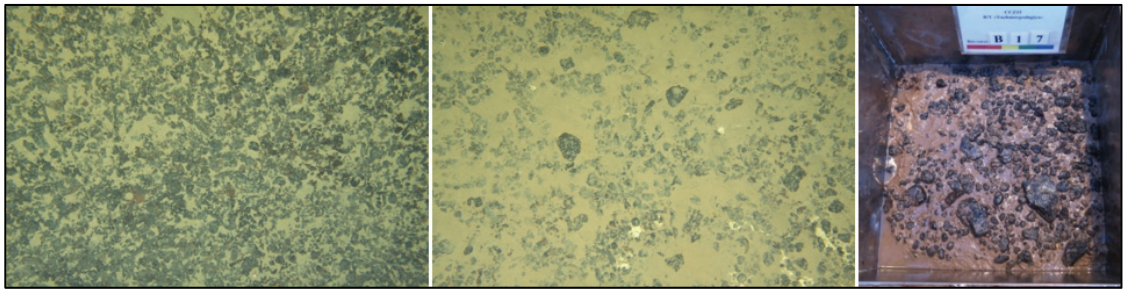

Photos: 2.4 x 1.5 m; L->R: F02 - 2015_08_17_094130, F02 - 2015_08_17_102520, B17 top-shot (box is 50 cm a side)

In addition to nodules, diagenetic processes can occasionally form crusts (Item 8). These are not likely to be minable using a collection system designed specifically to optimise nodule collection, but in any event are generally thought to be minor in extent within the TOML tenement areas. Diagenetic crusts were observed in ~ 0.02% of photos collected during the CCZ15 exploration cruise (Item 9).

7.5 Nodule mineralogy and chemistry

7.5.1 Nodule Fe-Mn oxide mineralogy

CCZ Nodules are understood to be mostly comprised of seven essential manganese and iron oxides, as well as minor accessory biogenic and rock-forming minerals.

Mineralogical descriptions are often confusing to the casual reader. This is due to inconsistencies in published identification of mineral components as a result of:

- The very fine grained to amorphous nature of the nodules;
- Some critical changes that can occur in mineral structure with heating and/or depressurization; and
- A related lack of consistency in naming of the manganese minerals amongst mineralogists.

Accordingly, essential manganese and iron minerals are summarised below:

Buserite is a 10 Å layered manganese mineral (phyllomanganate) that is likely the most important metal bearing phase in nodules. Buserite is not yet a formal mineral name so is not used by some mineralogists, however an application for recognition as a new name would “most probably be successful” (mindat.org). An issue with identifying buserite is that synthesised versions convert to birnessite at anywhere between room temperature and 200°C depending in part on cation composition (cations such as Ni^{2+}, Mg^{2+}, Ca^{2+}, and Co^{2+} tend to stabilize buserite). However, the peak transform temperature of nodule bearing buserite has been determined by differential thermal analysis to be at 120 to 130°C (Figure 7.38). Buserite can be referred to as “unstable” by mineralogists as it is distinguished from todorokite in XRD by a heating and reanalysis step.

Birnessite is a 7 Å layered manganese mineral that is often studied with buserite for use in fuel cells and prion and contaminated land remediation, due to ease in cation doping and mineral transformation. Unlike buserite it has one layer of interlayer crystalline water molecules (buserite has two) and is stable to about 200°C. Its abundance may have been overestimated in nodules in early (1970s) mineralogical work.

Vernadite is a name frequently used for “turbostratic” layered manganese minerals i.e., minerals such as buserite and birnessite are disordered along the basal plane with “big” molecular sheets turned into platelets that are barely discernible by electron microscope. Asbolane is another term sometimes used for disordered manganese minerals.

Todorokite is a 10 Å tunnel structured manganese mineral (tectomanganate) that is stable to about 600°C, some earlier researchers may have confused todorokite for buserite and it is likely relatively rare in nodules.

Goethite is a very common iron oxide on the earth’s surface. While pure crystalline goethite is stable to about 270°C (except for minor dehydration or dehydroxylation of surface iron (oxo) hydroxo functional groups at 200-250°C) it can grade into less stable poorly crystalline “gels” that are also difficult to identify and measure.

Feroxyhyte is an unstable high pressure form of goethite (i.e. it starts to breakdown once a nodule is lifted to surface). This may be the most important iron-mineral component of nodules. Its density is thought to be near-identical to goethite.

Lepidocrocite is a highly stable iron mineral. It transforms to maghemite at 250-300°C. It is more dense than goethite.

Key references for the above minerals are (Post, 1999; Frey et al, 2014; Johnson and Post, 2006; Novikov and Bogdanova, 2007; Wegorzewski and Kuhn, 2014; Choi et al, 2004; Burns and Brown, 1972; Ford and Bertsch, 1999; Haynes et al, 1985).

Figure 7.38 Generic model for transformations of manganese minerals in oceanic ferromanganese rocks during heating

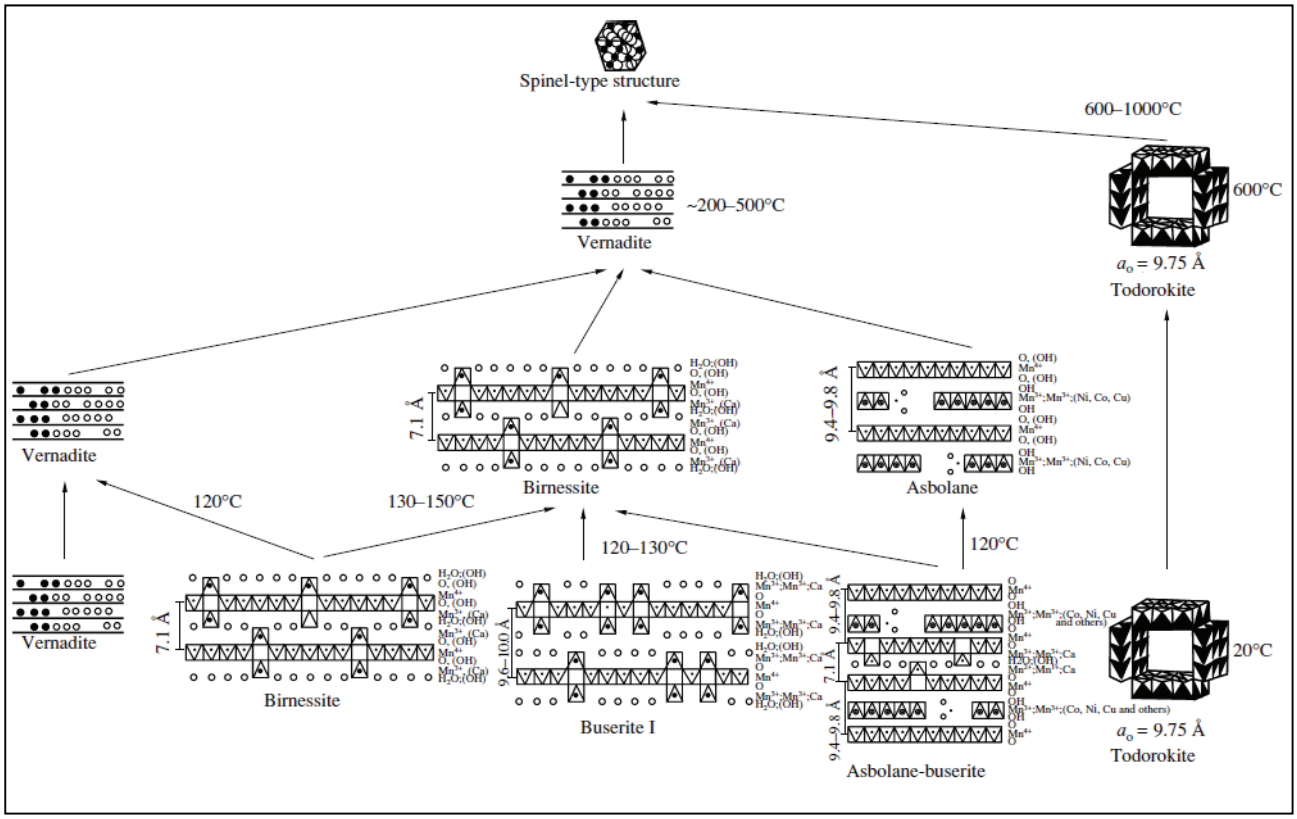

Source: Novikov and Bogdanova (2007)

Detailed studies and classification of the internal micro-textures of nodules include Choi et al (2002) and Wegorzewski and Kuhn (2014). The later classify two main layer types from an electron microscope study on nodules from the BGR area in the eastern CCZ:

- Layer type 1: dense layer with average Mn/Fe ratios of 1.80, average Ni + Cu of 0.81 wt.%, Co contents of 0.30 wt.% (interpreted as hydrogenetic metal precipitation from oxic waters). These layers consist of Fe-vernadite (δ-MnO_2) epitaxially intergrown with feroxyhyte (δ-FeOOH).
- Layer type 2: growth structures (dendritic growth structures and dense layers) with average Mn/Fe ratios of 96, Ni + Cu of 3.9 wt.%, Co contents of 0.08 wt.%, and a distinct Ni + Cu maximum of 6.51 wt.% at a Mn/Fe ratio of 56 (interpreted as suboxic-diagenetic, metal precipitation from suboxic pore waters). Type 2 layers mainly consist of turbostratic phyllomanganates such as 10 Å vernadite (buserite), 7 Å vernadite (birnessite) and todorokite are minor compounds.
- Mixed layer type 3: These layers can occur in the transition from layer type 1 to 2 or build-up of inhomogeneous growth structures. The Mn/Fe ratios of this material range between 3 and 11, Ni + Cu of 1 – 4.6 wt.%, and Co contents are between 0.02 and 0.77 wt%. In most cases these growth structures represent a mixture of type 1 and 2 layers.

See Figure 7.24 for examples of dense Fe rich layer 1 and dendritic Mn rich layer 2.

Wegorzewski and Kuhn (2014) estimate from the proportions of the two layer types that suboxic layers make up about 50 – 60% of the chemical inventory of the CCZ nodules whereas oxic-hydrogenetic layers comprise about 35 – 40% (i.e. a broadly similar outcome to the estimate for the central western CCZ in Glasby (2006).The remaining part (5 – 10%) of the nodules consists of incorporated sediment particles occurring along cracks and pores.

A feature studied by Novikov and Bogdanova (2007) is that of nodule modification. Specifically the mineral buserite is favoured by mineralogists for cation exchange experiments (e.g. for use as toxic metal accumulators) because the mineral is easy to dope with alternate cations. In the laboratory, a dust of buserite changes chemical composition within a few hours of being subjected to a solution of a particular cation (e.g. Na, Ca, or Ni). Novikov and Bogdanova (2007) also managed to increase nickel grades in samples up to 8% and copper up to 11%. While not specifically discussed by Novikov and Bogdanova (2007), it seems possible that nodule grades internally might change over time e.g. isotopic signatures reset (e.g. Ku et al, 1979), and grades change if the nodule moves past the CCD or enters a diagenetically active environment.

7.5.2 Other nodule mineralogy

Compared to the relatively small list of essential nodule forming minerals, McKelvey et al (1983) describe a very wide range of accessory minerals from Pacific nodules, which they classify into:

- Sheet silicates and zeolite minerals.
- Clastic silicate and volcanic minerals.
- Biogenic minerals.

These minerals are often not detected by X-ray diffraction methods on bulk samples because most exist as fine-grained crystallites similar to the manganese- and iron-phase minerals. McKelvey et al (1983) only found some of these minerals in concentrates after acid leaching although some minerals were identified by selective area electron diffraction.

These fine-grained hydrous aluminium silicates may have formed by submarine alteration (halmyrolysis) of the primary minerals in basalts or ash from transported from distant eruptions. These include chlorite, illite, kaolinite, montmorillonite, nontronite, pyrophyllite, and talc. The common clay present is generally montmorillonite. These minerals were probably incorporated from sediments during nodule growth.

The zeolites are authigenic (grew in place) and are found in cracks and cavities in the interior of nodules as well as sometime intergrown with the manganese oxides. The zeolites are hydrous silicates with a very open framework and large interconnecting spaces or channels that are filled with sodium, calcium, and variable amounts of water. They are mostly phillipsite with rarer analcite, clinoptilolite, epistilbite, erionite, and mordenite.

Clastic silicate and volcanic minerals occur as individual grains that may form the core or become incorporated into the nodule during growth. The more common clastic silicate minerals are quartz and various feldspars but there is a large number or trace and rare minerals, presumably all originally windborne

before settling to the seabed and incorporation. The volcanic minerals are barite, magnetite, anatase, ilmenite, and sphene.

Biogenic minerals include bones and teeth of fish, sharks, and whales (apatite, aragonite and calcite), and siliceous opaline skeletal remains (frustules) of some types of plankton, The debris such as bones and teeth are generally with the cores of nodules whereas the plankton remains are observed throughout the nodules and were probably incorporated during growth. The opaline debris in the interior of the nodule may undergo dissolution and be associated with the formation of phillipsite and secondary opal.

Opaline frustules are remains of plankton and are a major part of the host sediments for nodules. Plankton include phytoplankton (mostly diatoms and silicoflagellates), and zooplankton (mostly radiolarians) and the frustules are composed of hydrated silica ($SiO_2 \cdot nH_2O$; also called bSi or opal-A). The opaline silica is relatively disordered or amorphous (DeMaster, 2005), and it can dissolve in seawater/porewater and then reprecipitate as secondary opal-cristobalite/tridymite (also known as opal-CT or porcellanite). This occurs if for example there is saturation in terms of silica content in water and the accumulating ooze itself. While opal-CT is thought to normally only form at temperatures higher than typically found at the sea-floor (>50°C), Botz and Bohrmann (1991) use isotopes to confirm that opal-CT can occur at shallow burial depths and at temperatures of between 0 and 4°C (the CCZ seafloor is at a temperature of about 1.5°C).

Of interest as a stratigraphic marker amongst the biogenous oozes are Ethmodiscus silty clays, typically tens to hundreds of cm below the surface in the IOM area (Kotlinksi in ISA, 2010). This ooze is primarily composed of Ethmodiscus rex (E. rex), which is often referred to as a ‘giant’ diatom simply because of its unusually large size which can reach up to 1.8 mm in diameter. High concentrations of E. rex have been associated with seabed sedimentation during the Last Glacial Maximum period in seas of Asia (e.g. Xiong et al 2015). A common strategy of E. rex is to migrate down from the photic zone into the water column for up to two weeks at a time in search of ‘dark nitrate’ (Villareal and Carpenter, 2004).

Of note are salts that are the result of precipitation from contained seawater, namely are sylvite, halite, and other common evaporites. These residues are also the primary source of the anions-borate, bromide, chloride, fluoride, and iodide in manganese nodules.

McKelvey et al (1983) mention that several elements are associated almost entirely with the accessory minerals of the nodule discussed above. These are Al, Cr, K, P, and Si. Other elements associated with the accessory minerals and possibly with the Fe-Mn phases are Ba, Mg, Na, and Zr.

7.5.3 Sediment mineralogy

The geology of the sediments in the CCZ (morphology, stratigraphy and composition) is dealt with earlier in this section. In Figure 7.2, the ISA (2010) compilation of surficial sediment types (from a number of contractors) shows them to be distributed roughly perpendicular to the fracture zones, trending from mostly biogenic carbonate sediments in the south to south-southeast, to biogenic siliceous ooze in the central regions of the CCZ, to inorganic muds in the north to north-northwest. The transitions between sediment types also closely mimic the position of the Clarion and Clipperton fracture zones. Figure 7.39 summarises whole sediment mineralogy from the IOM area which is thought to be fairly typical of most of the TOML areas that are nearby.

Not surprisingly, all of the minerals present in Figure 7.39 are the same types as discussed above for the nodules. Their proportions are, however, very different. Biogenic opal now being the most important, with abundant salt (surface sediments have water contents typically well over 100%; mass of water over mass of soil solids), a range of clastic minerals and only minor (~5%) ferro-manganese minerals, which in parts of the TOML area were visible as fine black disseminated mineral grains grading to micronodules (<2 mm in diameter).

It is notable from Figure 7.39 that there is next to no difference in mineral proportions between the three layers down to 10 cm.

Figure 7.39 Minerals in the geochemically active layer within the IOM area, excluding large nodules

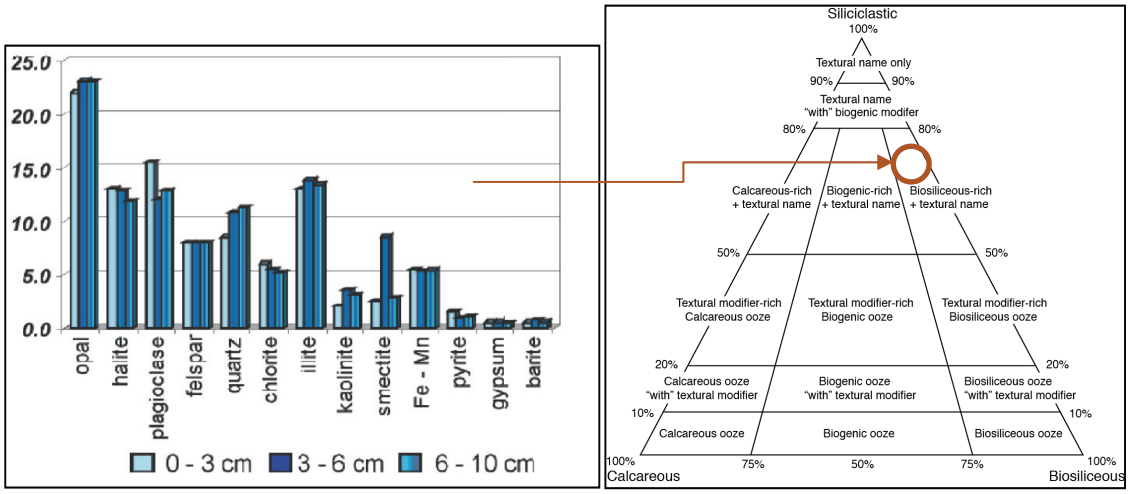

Source: ISA (2010)

When the relevant mineral components are plotted on the sediment classification system of Li et al (2015), the proportion of siliclastic minerals to opal classify it as biosiliceous rich sediment rather than an ooze in the strict sense (Figure 7.39).

7.5.4 Nodule chemistry

Item 9, Item 12 and Item 14 detail the exploration results that support the mineral resource, but other key chemical characteristics are presented here.

Figure 7.40 Modelled Mn and Cu grades in nodules across the CCZ

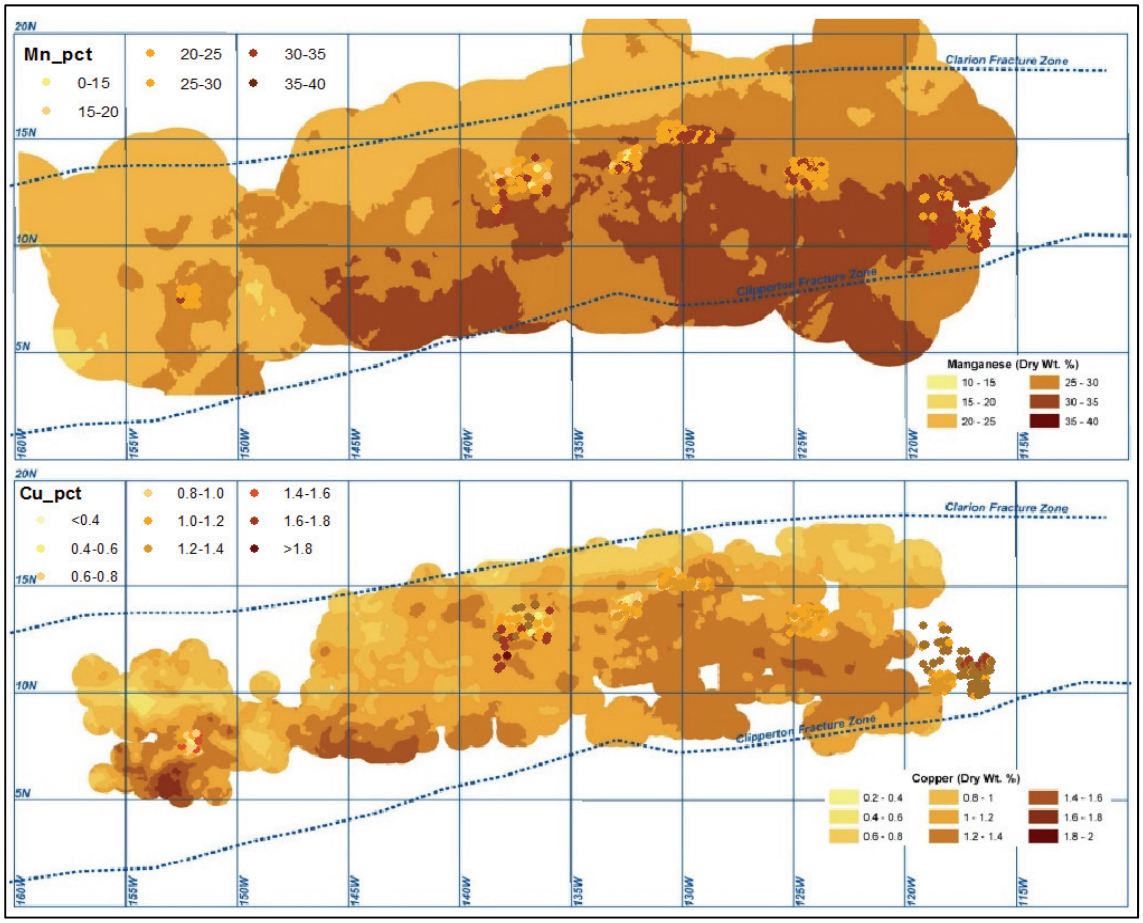

Source: Morgan (2009), point data attributed to OMI

Grade variation through the CCZ is well summarised by ISA (2010) and Morgan (2009) who combined datasets provided by several of the ISA contractors.

Within the CCZ nodule field, nodule chemistry varies only slightly compared to the differences in mean nodule grades from other basins elsewhere in the world (Table 7.1). The strongest trend is observed for Mn and Cu, which both increase towards the southeast (Kazmin in ISA, 2003; ISA, 2010; Morgan, 2009; see Figure 7.40). This may relate to a slightly more sub-oxic diagenetic history of nodule formation or perhaps to proximity to metal sources from the East Pacific Rise or the American continents.

In contrast, Ni and Co partly correlate along the central axis of the CCZ (Figure 7.41), with the Co appearing to be offset to the north from the Ni. The reason for the distribution of these metals is unknown, but may relate to a lack of competition for the metals in the sediments, which have both lower chlorite and lower smectite in this region (Futterer, 2006).

Figure 7.41 Modelled Ni and Co grades in nodules across the CCZ

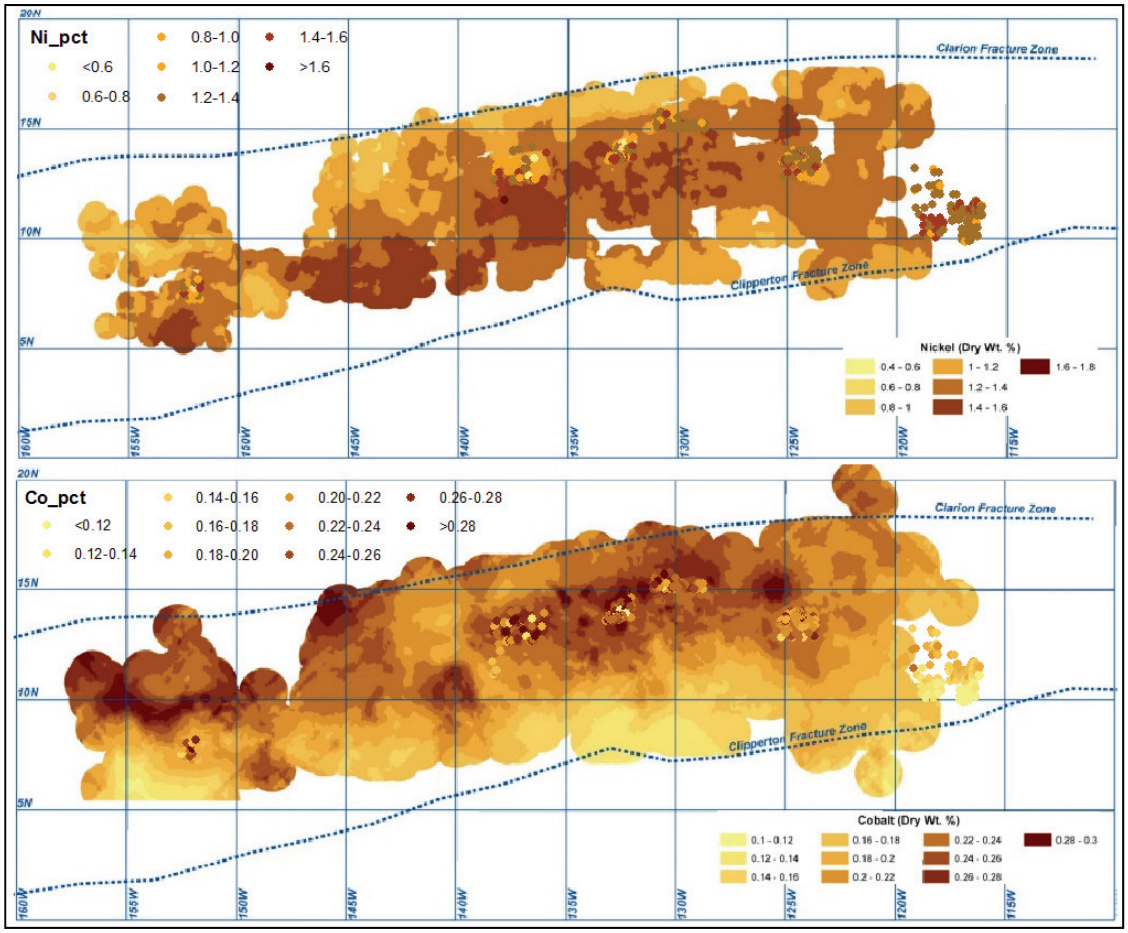

Source: Morgan (2009), point data attributed to OMI.

Unlike the data supplied by the ISA, dredge samples collected during the CCZ13 and CCZ15 cruises by TOML were analysed for iron. This allowed for plotting the data on genetic discrimination diagram of Bonatti et al (1972). Figure 7.42 shows that:

- The nodules of the TOML CCZ area compare consistently with the average published CCZ value of Hein and Koschinsky (2013).
- Ferromanganese crusts dredged during the TOML cruises plot as diagenetic compared to the Pacific Prime crusts of Hein and Koschinsky (2013), although some have sediment inclusions that result in low Fe and Mn and plot to the left of the main ferromanganese trend
- One nodule sample from TOML Area A (sample A (D02)) looks to be more hydrogenetic in nature than the others.

Figure 7.42 Nodule discrimination plot with TOML dredge samples

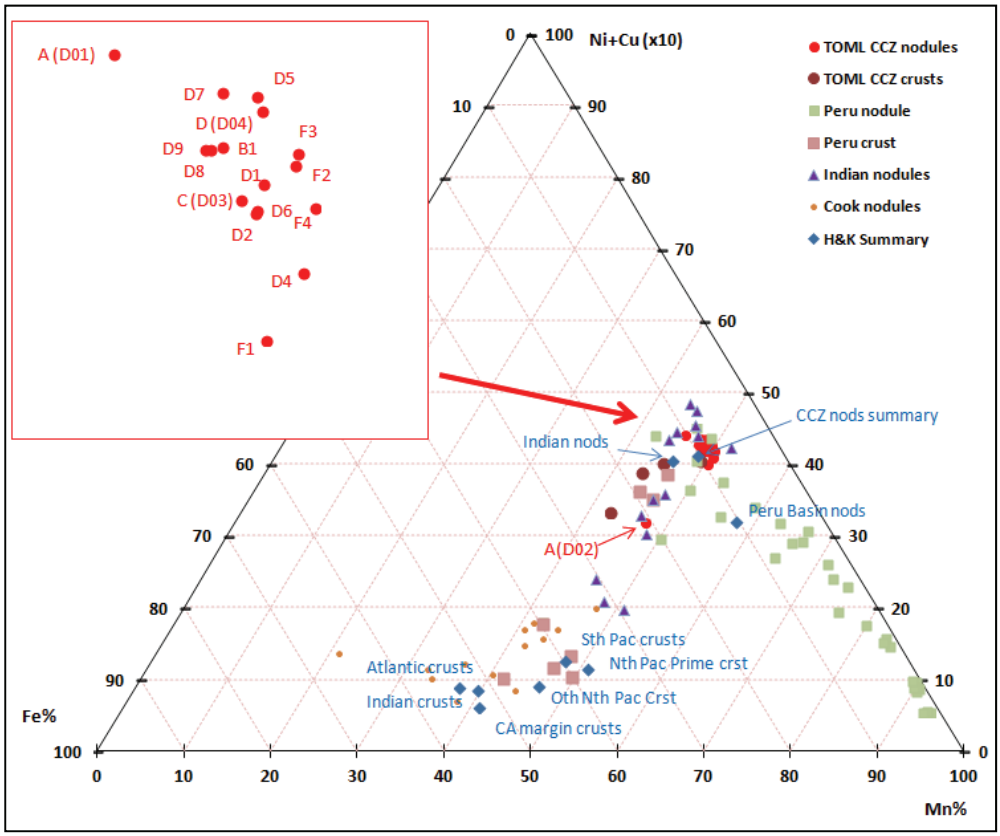

Modified after Bonatti et al, (1972); Peru Basin data from von Stakelberg 1987, Indian Ocean from Pattan and Parthiban 2011, Cook Islands from Glasby et al 1983, summary points from Hein and Koschinsky 2013

7.5.5 Grades of other metals

Grades for elements other than Mn, Ni, Cu and Co are not reported in the mineral resource (Item 14) for the TOML tenement area. Boxcores from CCZ15 cruise where analysed for a range of metals (Item 9), and these broadly agree with grades for a wider range of metals reported on Pacific nodules by McKelvey et al (1983), except for Rare Earth Element (REE) which are lower in the TOML dataset (see below). McKelvey et al (1983) do not separate out the grades of nodules from the CCZ but document average grades for nodules with Ni+Cu >1.8%, the bulk of which come from the CCZ. These are summarised below per the classification of McKelvey et al (1983) with their average grade followed by the average grade determined by TOML:

- Other base or alloy metals such as Zn (0.14%; 0.147%), Mo (0.039%; 0.064%), Ti (0.58%; 0.301%) and Pb (0.071%; 0.019%)
- Rare earth elements and other transition metals such as Sr (0.077%;0.057%), Y (0.012%; 0.009%), Zr (0.027%), Te (0.021%), La (0.019%; 0.012%), Ce (0.066%; 0.029%) and Nd (0.023%; 0.013%)
- Possible deleterious elements or reagent consumers and enhancers such as F (3%), Mg (1.57%; 1.94%), Al (2.96%; 2.47%), Si (8.26%;6.82%), S (0.319%; 0.13%), Cl (0.860%), Ca (1.73%; 1.76%), As (0.012%; <0.005% in some analysed dredge samples), and Ba (0.224%; 0.284%)

These levels of metals are supported in some cases (Zn, Mo) by data presented by Haynes et al. (1985), who also reported very limited data on Au and platinum group metals (all at the ppb level except Pt which averaged 0.1 ppm from 5 samples).

The REE values in the TOML tenement areas more closely agree with those published from the historical Lockheed Martin Exploration Area by Spickermann, (2012). This area is adjacent to TOML Exploration Areas B, D, and E. Total REE reported by Spickermann is about 0.08% (0.079% from TOML Areas A, C, B, D and F) with a median of 617 (619) ppm light REE (La-Eu) and 171 (180) ppm heavy REE (Gd-Y).

Also of interest is a clear trend of increasing Ba and S from TOML Area A, B and C to D and then to F. This trend suggests increased barite ($BaSO_4$) whose presence in turn is thought to represent increased primary

productivity (or rather activity) within the diagenetic environment (Ba preferentially captures S released from decaying organic material in the sediment below the calcite compensation depth (e.g. Schulz and Zabel, 2006). This trend corresponds well with modern sea surface primary productivity (Figure 7.2).

7.5.6 Nodule abundance and estimation of tonnages

A key feature in the vertical distribution of nodules in the CCZ is that the majority appear to be located either on the seafloor or immediately below it (<10 cm from the surface; Item 8). This feature means that effectively estimating nodule abundance and nodule mining (or collecting) is a two dimensional problem. To date, this is how all of the workers in the CCZ have worked on the question of nodule abundance. All of the nodule miners/collectors known to have been designed to date (Item 6) also follow similar principles by scraping, sucking, plucking or jetting nodules off the seafloor (± semi-liquid layer).

Nodule abundance is estimated either by:

- Taking a sample from the seafloor and dividing the weight of nodules by the area of the primary sampler (Section 9.3);
- Using a photograph of nodules on the seabed to estimate their individual weight (e.g. as used by Kennecott; Felix 1980) which has been used with considerable success in some areas by TOML (Items 9 and 12) and dividing the weight of nodules by the area of the image; or
- Using sonar response to estimate percentage coverage of the seafloor by nodules and converting this to abundance using calibration factors (e.g. as used by COMRA; ISA, 2010). Ruhlemann et al. (2011) discuss some of the issues with this approach for example the interplay between nodule size, nodule abundance and response to acoustic surveys (e.g. backscatter). TOML has also observed a relationship with host sediment type that complicates estimations of abundance using acoustic methods (Item 9).

An alternative method more commonly used in land based deposits is to derive a three dimensional model involving volume and density. This has a number of inherent problems with regards to CCZ nodules:

- Depth of penetration of the samplers is usually not measured, and the relative depth of the semi-liquid layer versus the clay layer is usually not measured. Thus these would have to be estimated or assumed to a low degree of certainty.
- The order of the depth is trivial i.e. approximately $1x10^{-5}$ that of the inter-sample distance (i.e. 0.1 to 0.3 m against 10 to 30 km spacing).
- Densities of the sediment would need to be estimated or assumed, again to a low degree of certainty.
- It is unlikely that the proportion of sediment is critical in any mining/collection operation, as engineering for nodule collection would minimize sediment collection and aim to separate and discard any adhering sediment as early in the collection process as possible because it has no known economic value, and for environmental reasons is best left in-situ. Speed over ground for the collector, nodule size and wet density of the nodules are the factors that most likely would drive the fundamentals of a collection and transportation system (Item 6).

Nodule abundance is typically reported in wet kg/m^2 for similar reasons:

- Wet weights are the most relevant in any collecting and transport operation;
- Often the nodule samples have multiple uses once collected at sea, some are for assay, others for environmental or metallurgical test work and some for reference (retaining the sample to dry and then weigh is less convenient);
- With complexity related to drying conditions and determining wet/dry density, weighing of the samples at surface is the simplest and most effective way to measure and compare nodule abundances between different cruises and between the different contractors (Item 9).

As discussed in Item 11, sample aliquots were dried, crushed and pulverised before assaying. Using dry weight percent assays on wet weight mineral resource and inventory is a commonly accepted practice for similar bulk commodities that can contain significant amounts of free water (e.g. iron ore or Ni-Co laterite).

Data analysis in Item 9 shows that nodule abundance variability is significantly higher than metal grades in most areas, suggesting that abundance estimation will be the key variable of uncertainty in mineral resource estimation. Figure 7.43 shows evidence of this compared to Figure 7.40 and Figure 7.41.

Figure 7.43 Modelled nodule abundance across the CCZ

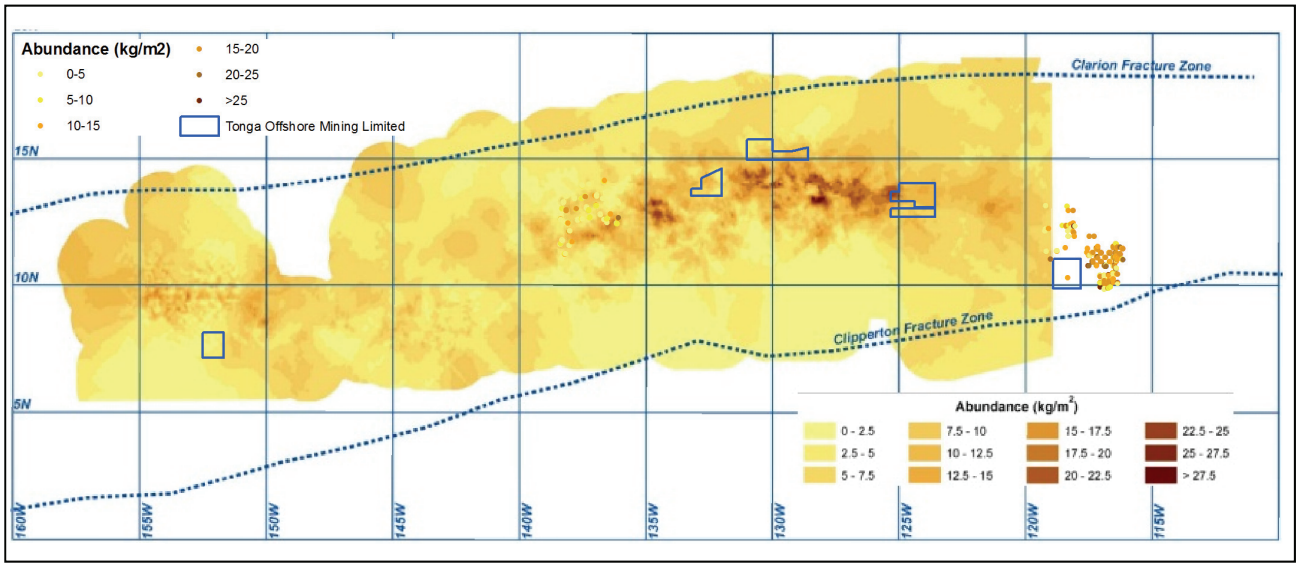

Source: Morgan (2009), point data attributed to OMI.

Nodules have a clear relationship between long axis length and weight as discussed in section 12.2. For nodules exposed at the seafloor it is thus also possible to accurately estimate abundance from photographs.

7.6 Nodule Density and Moisture Content

7.6.1 Nodule density

Polymetallic nodules have an average wet density of about 2 t/m^3 (Table 7.7; Figure 7.44). TOML confirmed historical results from the north Pacific (Hessler and Jumars, 1974) through ~ 60 water displacement density measurements. The density measurements were done for both single nodules and for nodules in bulk, including fragments and sand resulting from attrition during transport and handing.

The results are similar except that the mean of the single nodules is ~ 2.8% lower than that of the bulk measurements. This might be due to air or water filled expansion cracks in the single nodules (that were collected ~7 months before the density measurements were made) the bulk nodule samples contained many more fragments that presumably relate to fractures along these cracks. The bulk nodule measurements are preferred over the single nodule measurements as they are likely more accurate due to larger sample size. The bulk nodule measurements also have a lower standard deviation.

Also noted is that Area F nodules might be slightly less dense than the other TOML tenement areas (Table 7.7; Figure 7.44). By averages this is of the order of 2 - 4%, being slightly more pronounced in the single nodule estimates. Nodule densities have not yet been measured for Area A.

Table 7.7 Nodule Density measurements TOML Area B, C, D and F

		g/cm3					
	Count	Min	Median	Mean	Max	Range	Standard deviation
Single nodules	34	1.78	1.95	1.95	2.38	0.60	0.11
Bulk nodules	27	1.94	2.01	2.01	2.07	0.13	0.03
Single nodules area F	9	1.83	1.91	1.90	1.99	0.16	0.06
Bulk nodules area F	6	1.94	1.97	1.97	2.01	0.07	0.02

Figure 7.44 Nodule densities of samples from TOML areas B-D, F and central north Pacific

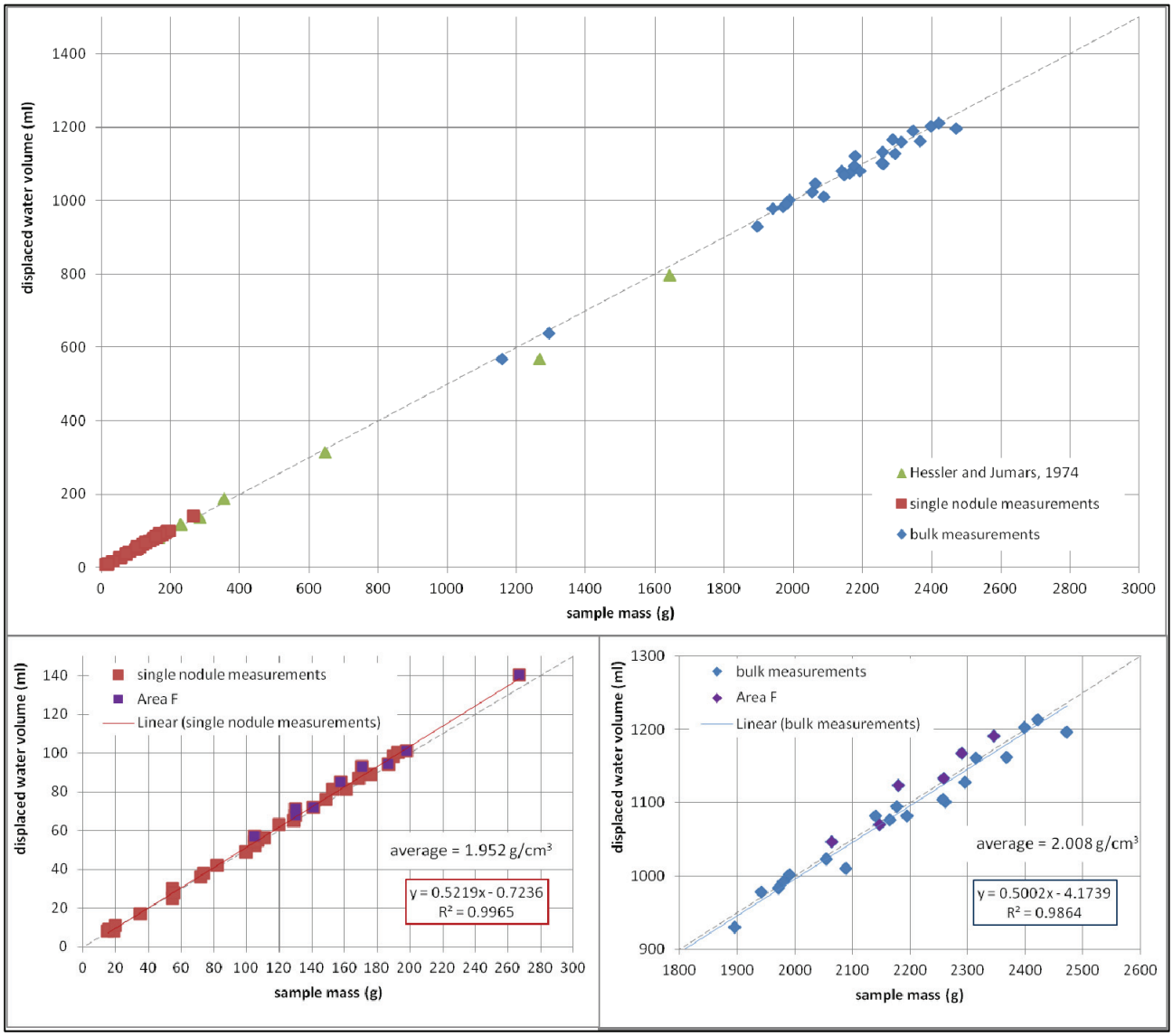

Single and bulk measurements from nodules collected during the CCZ15 cruise; historical values from Hessler and Jumars (1974)

7.6.2 Nodule water content

Exploitation of polymetallic nodules is likely to be done on a wet tonnage basis in that nodules will be transported, stored and sold without oven drying. In exploration, the abundance of nodules collected by free fall grabs or box-corers is also typically measured on the exploration vessel immediately after collection before the sample has time to air dry (Item 9). Reporting a polymetallic nodule mineral resource on a wet basis is thus simpler and more appropriate than reporting on a dry basis, as is done for grade.

Total water content in wet nodules is estimated at 44% (Table 7.8), but the situation is further complicated as two main types of water are present:

- **Water of crystallization** included within manganese and iron oxide minerals. This was determined in TOML test work to consistently be about **16%** by wet weight (including other likely trace levels of other volatiles). A very small amount of water of crystallization likely starts being removed at temperatures as low as 50 - 70°C through a transformation of the manganese mineral buserite into birnessite, but most is stable until much higher temperatures (115°C and greater; Novikov and Bogdanova (2007); Figure 7.38).
- **"Free" water** included within pores and other cavities within the nodules including water adsorbed onto minerals – this is estimated to be around **28%** by wet weight depending on the micro and macro

void space in the nodules. Air-drying may remove approximately 16% (absolute) of this, with the rest by oven drying (up to 105°C).

Estimating the water content is then complicated further again due to two properties specific to the nodules:

- The nodules have very high porosity (~50%; Ifremer, 2010) and are hygroscopic (Figure 7.45). Within a day of drying to 105°C pulped nodules will absorb at least 7% of moisture by mass if exposed to ambient air.
- Depressurization of the nodules after collection leads to mineral transformation (e.g. breakdown of feroxyhyte) and micro-fractures and fractures. Free water might be added into the cracks and micro-cracks. TOML tests suggest that four months after collection about 3% free water on a wet basis can be added into samples that are soaked in water (this 3% is not included in the totals indicated above).

Published moisture values from the very comprehensive metallurgical reports by Haynes et al. (1985) and Fuerstenau et al. (1973) are summarised below along with TOML results.

Table 7.8 Comparison with published moisture contents

Source	Total Moisture	Free Moisture	Water of Crystallisation
Mero (1965) p233	–	30-36*	–
Fuerstenau et al. (1973)**	>22.66%	13.1%	>8.74%
Haynes et al. (1985)	45-50%	35–45% with about half able to be dried in air	5-10%
Wiedicke-Hombach et al (2012)	44%	Not specified	Not specified
TOML measurements	44%	28% with about 60% of this able to be dried in air	16%***

* drying temp not specified may include some water of crystallization; **used in the 2012 Nautilus CCZ NI43-101 report (Golder, 2013) to characterise moisture; *** includes ±2% water of crystallisation lost up to 105°C

Figure 7.45 Nodule sample (pulp) absorption after drying to 105°C for 6 hours

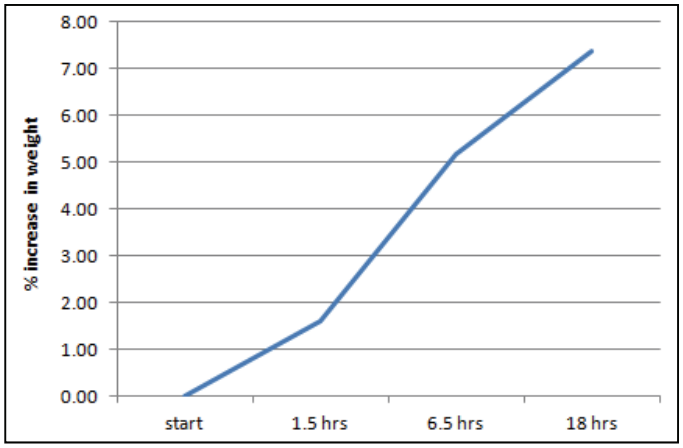

Test work done by TOML on select nodules involved three stages of drying.

Stage one was air drying at up to 260 hours at ambient temperatures of 22°C to 25°C and humidity of 50% to 60% (Figure 7.46). Moisture content lost by the time of stabilisation (around 200 hours at these ambient temperature and humidity) varied between 13% and 19%.

Figure 7.46 Air drying results for a short term sample batch (L) and a long term sample batch (R)

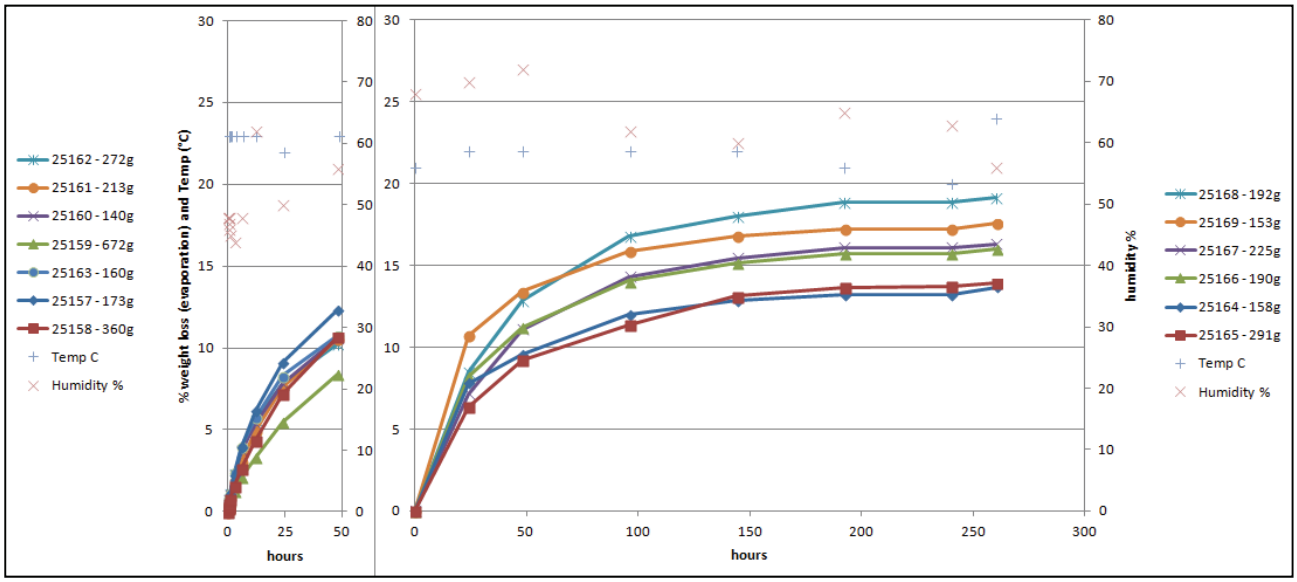

Stage two was oven drying at up to 978 hours in seven temperature steps. From Figure 7.47 the moisture content lost was a very consistent 15% to 16.5% at 105°C and 18% to 19.5% at 160°C.

Figure 7.47 Oven drying results for nodules

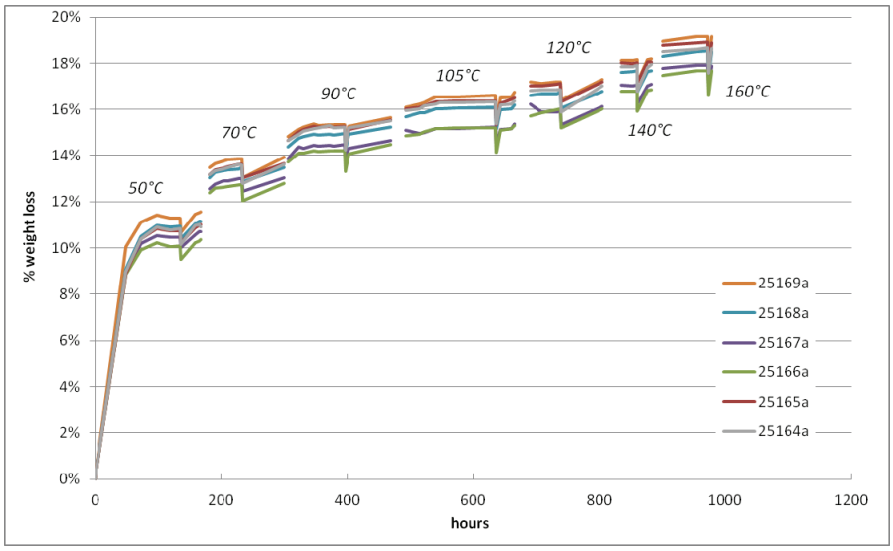

Between each oven drying temperature the samples were left exposed to ambient air for one hour to measure hydroscopic weight increase. Whole nodules absorbed water more slowly than pulverised nodules (e.g. Figure 7.45).

Stage three was loss on ignition (LOI) where samples were pulverised and effectively sintered at 1,000°C, driving off all moisture that might include other types of "combined water" (hydrates and labile hydroxy-compounds) and carbon dioxide although the latter is thought to be minimal in nodules.

From Figure 7.48 the LOI from 160°C was remarkably constant for the test samples between 14% and 15.2% which equates to:

- 10.6% to 11.8% from 160°C on a starting wet basis.
- 16.8% to 18% from 105°C. The results are comparable with other TOML analyses and figures from some sources:
  - Mero (1965) reports LOI (1100°C) of 15% to 39% averaging 25.8% but from nodules at an “air dried” level.

— Reference material CGL131 (a nodule standard from the eastern German area in the CCZ) averaged an LOI of 16.98% from 16 laboratories, although the figure is not certified

Other workers report higher LOIs (20% to 25%) but do not specify the drying method in enough detail for valid comparison. The chance of hygroscopic absorption of moisture cannot be discounted.

Figure 7.48 Loss on ignition (at 1,000°C) for two batches of TOML samples

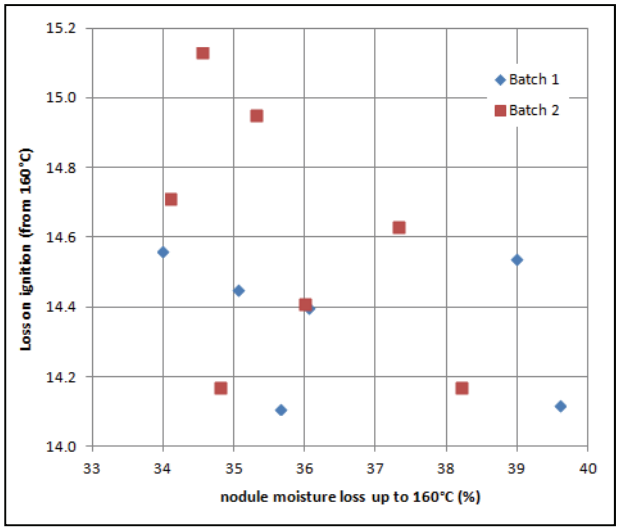

A combined drying curve is summarised in Figure 7.49. Average total moisture content is 47% with most of the variance in total moisture apparent from the earliest stages of air-drying (48 hours at ambient temperature). With consideration of ~3% storage water absorbed into post sampling expansion cracks (see above) a standard total moisture content of 44% is derived.

Figure 7.49 Three stage drying curve for polymetallic nodules

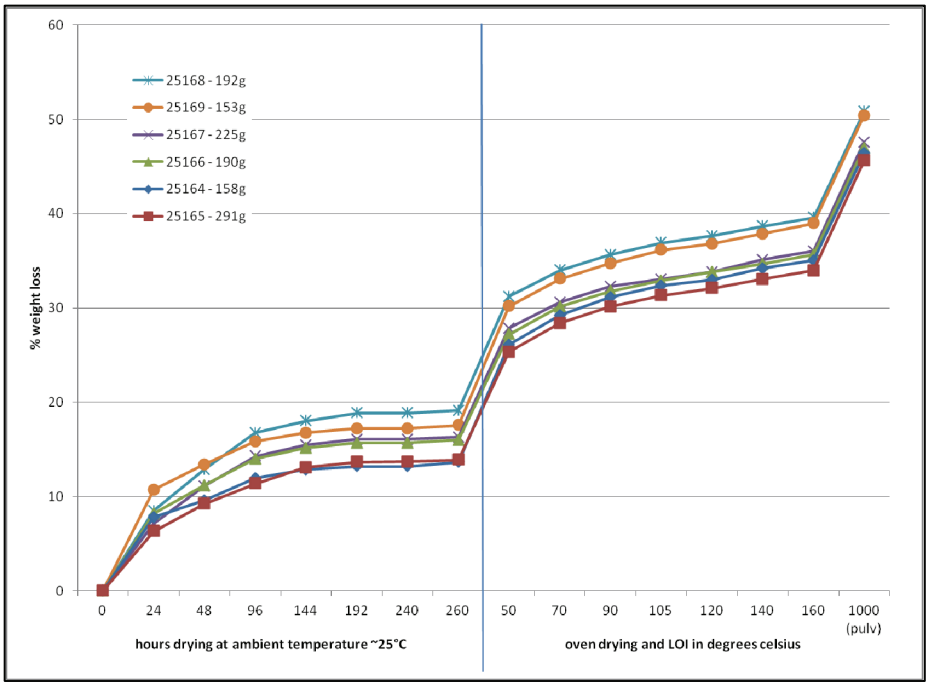

Average total moisture content is 47% with most of the variance in total moisture apparent from the earliest stages of air-drying (48 hours at ambient temperature). After adjustment for absorbed water (determined in a separate test involving samples sealed from collection and sampled soaked before drying) an effective moisture content of 44% is arrived at.

In the estimation of moisture content (or other component; e.g. Figure 7.50) **wet basis** is taken before any air drying or soaking, **dry basis** is taken at 105°C and a **volatile free basis** is taken after LOI at 1,000°C with all volatiles removed. Other bases are mentioned in the text with the temperature specified.

Figure 7.50 Bulk nodule composition on a wet, dry and volatile free basis

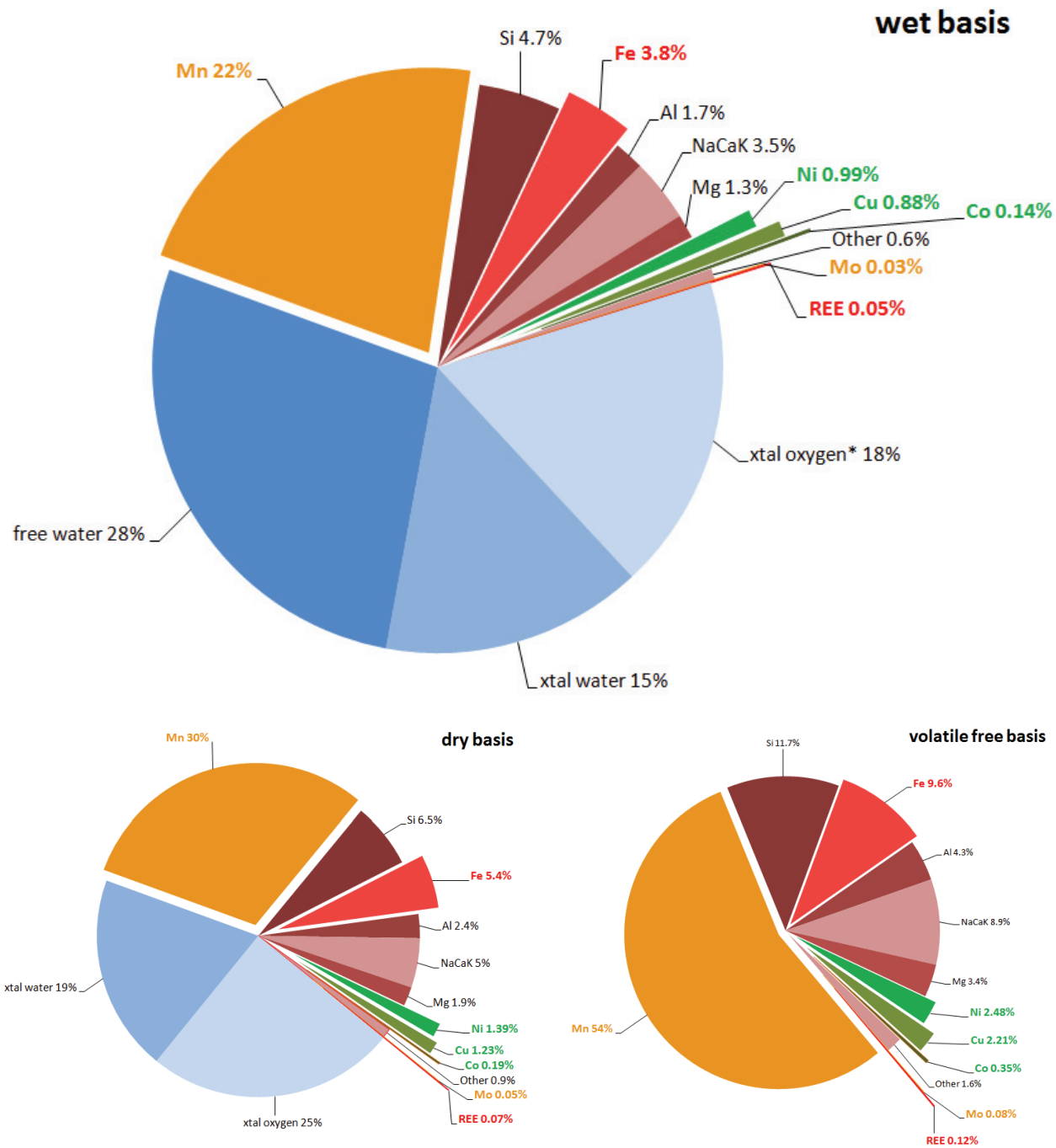

Notes: Based on average grades of dredge samples collected during CCZ13 so may not be representative of all or part of the mineral resource for the TOML area. *A minor amount of oxygen of crystallisation may have been added or removed as a consequence of the XRF analytical process. The sintered composition shown is theoretical and does not, for example, consider partial reduction or addition of reductant or flux. Xtal water is water of crystallisation also known as interlayer water. Xtal oxygen is stoichiometric oxygen in the mineral structures.

7.7 Diagenetic Crusts

The minor amounts of ferro-manganese crust found in the CCZ are not the same as hydrogenetic cobalt-rich crusts typically found on the top of seamounts e.g. in the Pacific Prime Zone in the north-west Pacific Ocean (e.g. Hein and Koschinsky, 2013).Two types have been logged, both by TOML and other workers (e.g. Ifremer; Menot et al., 2010):

- Massive crust is five to ten centimetres thick and is typically found in blocks several decimetres a side (e.g. Figure 7.51, Figure 7.54, Figure 7.55), but occasionally as pavement (e.g. Figure 7.53); and
- Crustal-nodules are small to medium sized (<20 cm) discrete fragments of ferro-manganese (e.g. Figure 7.53) that can grade into nodules (e.g. Figure 7.56).

In total, crusts were logged in ~0.6% of the photo-profiles, with crustal nodules more common (~0.5%) and massive crusts being present only ~0.1% of the time. Neither type was collected in box-cores during the TOML CCZ15 cruise, and their extent is deemed insignificant in terms of the mineral resource estimation in Item 14.

The massive crust clearly forms into the sediment with preserved casts of worm burrows. It is possible that they form in horizons below the surface as fragments often (but not always) are found in lines (Figure 7.54, Figure 7.55) and as suggested by a sub-surface reflector seen during just before a dredge landing that captured some massive crust (Figure 7.51).

Figure 7.51 Crust and possible related acoustic signal

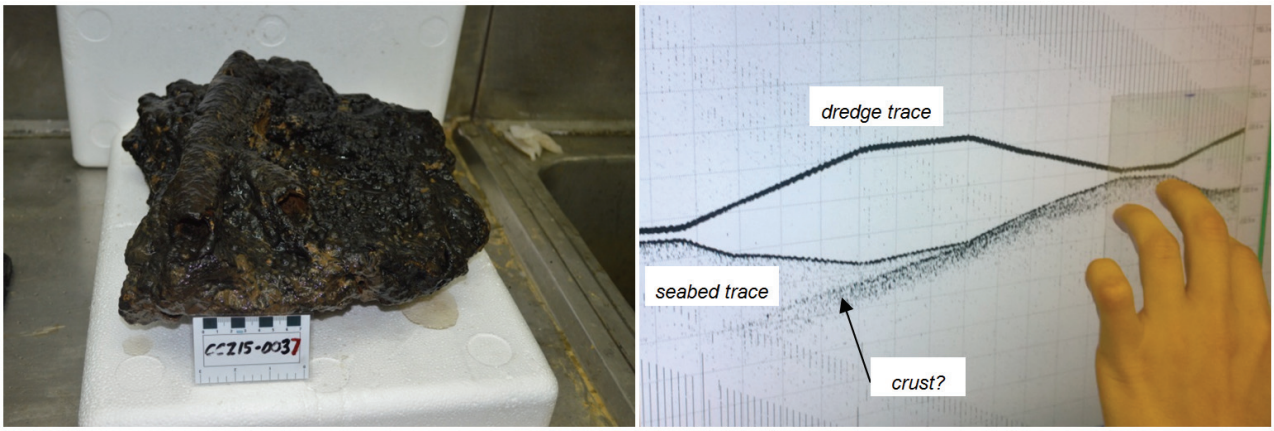

Worm tube cast in large crust fragment dredged from Area A (sample D01) and acoustic pinger trace from the same dredge that can be interpreted to show a sub-surface crust. Note that Area A sample D02, taken 40 km away from D01 did not contain any crust fragments.

Figure 7.52 Distribution of crust photos logged during CCZ15

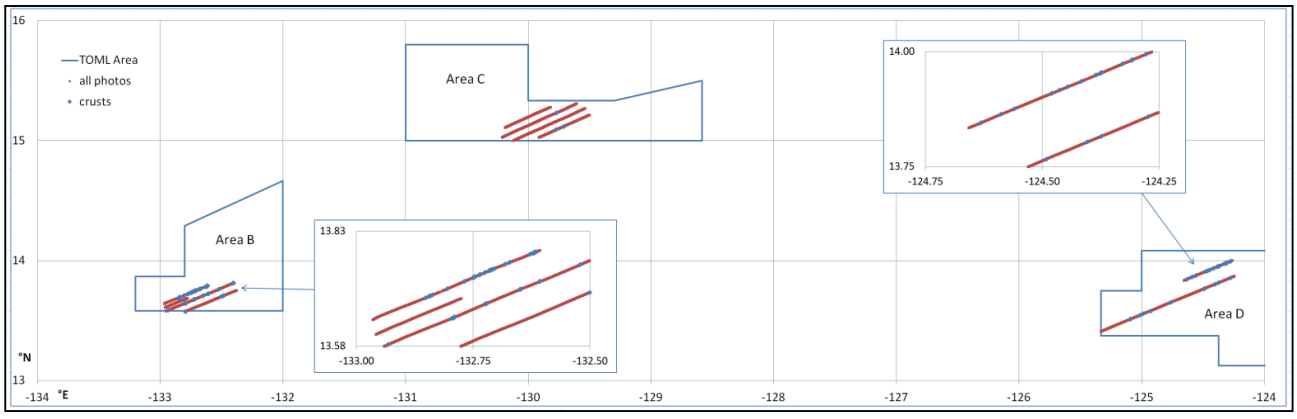

Figure 7.53 Graded crust fragment, photos of crust types from the Nautile, and brown veins in soft crust

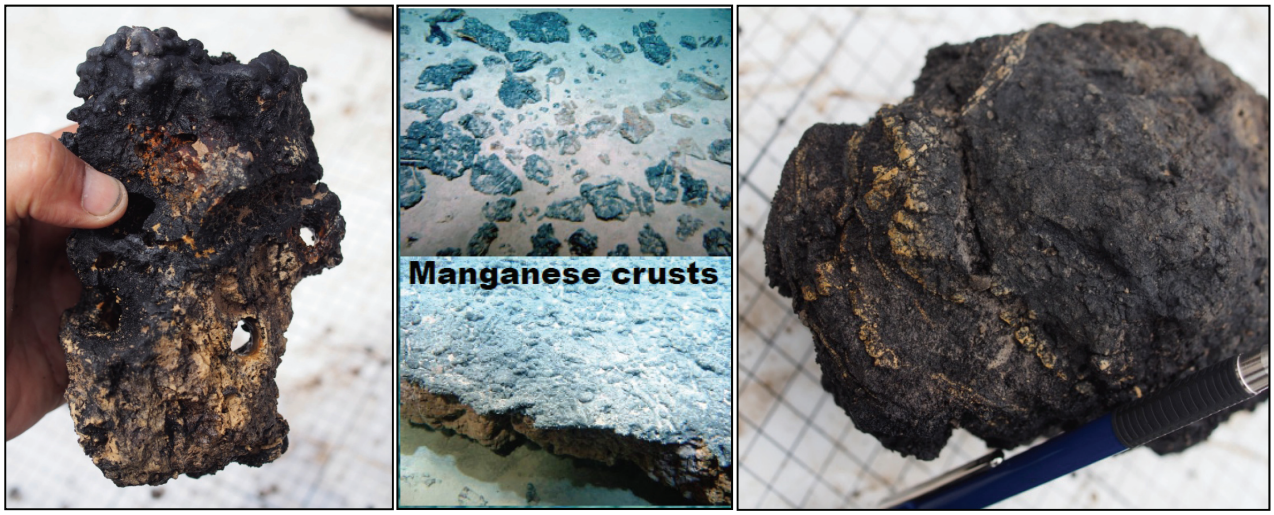

Graded fragment from CCZ13 dredge D04 in Area D, with dark nodules at top (upper part of photo) and more brown mud rich lower section with worm burrows (benthic mud washed out); pictures of crusts from Menot et al, (2010); Brown veins interpreted to be barite in manganese indurated sediment (diagenetic crust) – sample CCZ13, D06

Figure 7.54 Examples of massive crust fragments Area B

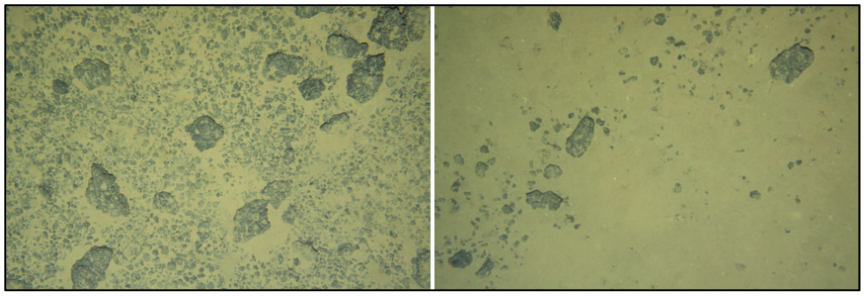

Photos: 2.4 x 1.5 m; L->R: F02 - 2015_08_16_190630 F02 - 2015_08_17_073523

Figure 7.55 Examples of massive crust fragments Area D

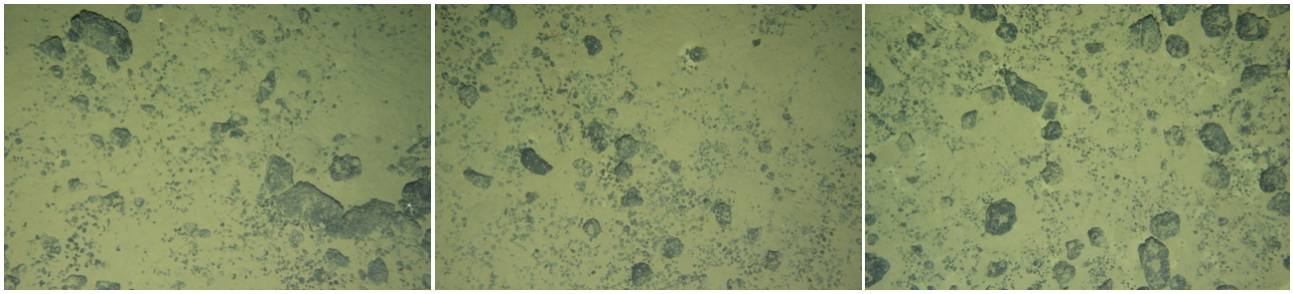

Photos: 2.4 x 1.5 m; L->R: F10 - 2015_09_16_182431; F10 - 2015_09_16_184605; F10 - 2015_09_16_185038

The crustal nodules are likely to form much like nodules do but perhaps form in areas with very thin geochemically layers as they can grade into nodules (Figure 7.56). Alternatively they may form in areas with lots of seeds (e.g. from deposited volcanic ash) or from layers of reprecipitated opal as they are similar in some ways to rare orange-brown crust interpreted to be opaline and observed during the CCZ13 cruise (Figure 7.57).

A third crust-like material that is very rarely encountered is zeolites. Venkatarathnam and Biscaye (1973) describe these as forming from halmyrolysis (subsea diagenetic alteration) of both volcanic material (probably ash within the CCZ) and likely from opal rich sedimentary material. Thin sheets of zeolite crust were identified in the photo-profiling in just a few locations in Area B (e.g. Figure 7.58), and in one location in Area D.

Figure 7.56 Nodules grading to surface crustal-nodules Area B

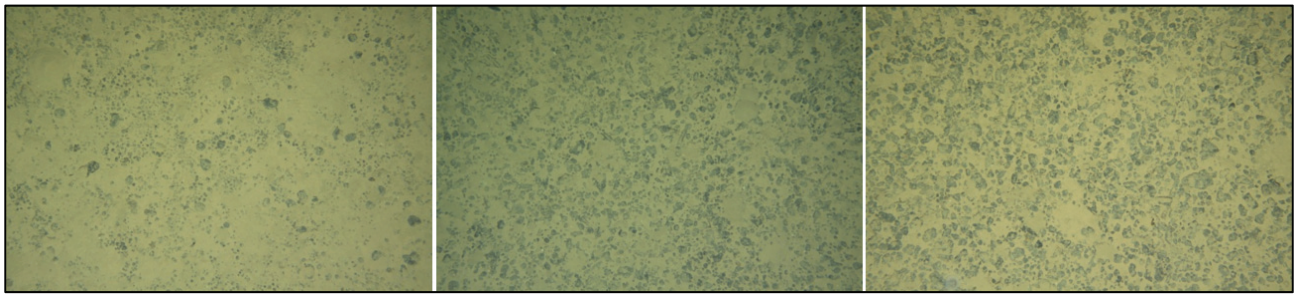

Photos: 2.4 x 1.5 m; L->R: F02 - 2015_08_17_005754; F02 - 2015_08_17_010443; F02 - 2015_08_17_010044

Figure 7.57 Ferromanganese coated crust interpreted to be opaline

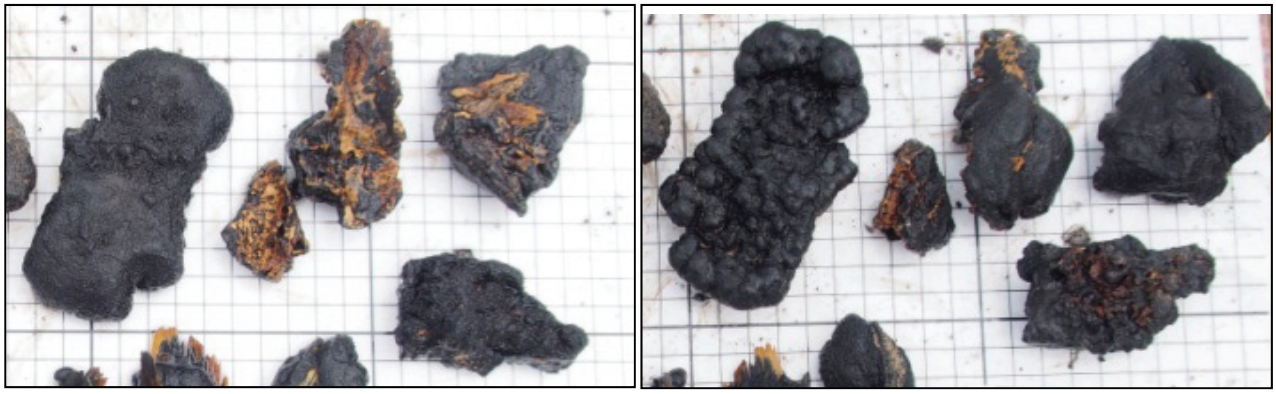

Collected in CCZ13 D08 in Area D; photos are of each side; large squares are 10 cm

Figure 7.58 Zeolite crust on carbonate, Area B

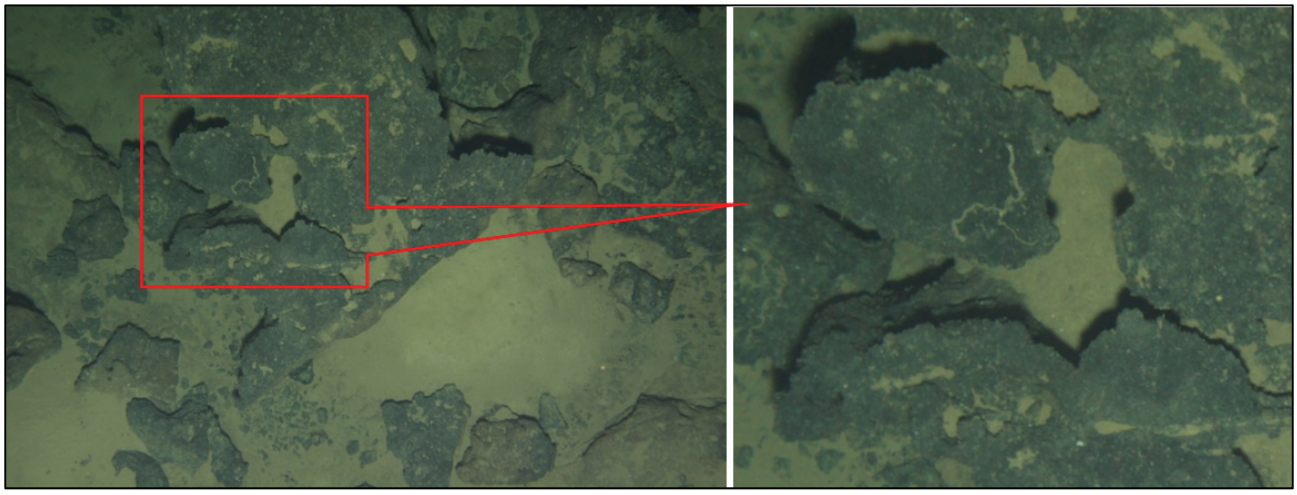

Photo at left: 2.4 x 1.5 m; F02 - 2015_08_17_054645